ACS APPLIED ELECTRONIC MATERIALS

pubs.acs.org/acsaelm Article

Carrier Dynamics in Thin Germanium−Tin Epilayers

Ernest Rogowicz,* Jan Kopaczek, Joanna Kutrowska-Girzycka, Maksym Myronov,* Robert Kudrawiec,* and Marcin Syperek*

Cite This: *ACS Appl. Electron. Mater.* 2021, 3, 344−352 Read Online

ACCESS | Metrics & More | Article Recommendations | Supporting Information

ABSTRACT: The Si-based mid-infrared photonics is an emerging technology in which group-IV germanium−tin ($Ge_{1-x}Sn_x$) binary alloys can play a fundamental role in the development of a Si-compatible photonic components including monolithically integrated coherent light sources and detectors, on the same Si or SOI substrate. Although the $Ge_{1-x}Sn_x$-on-Si lasers, at low temperatures, have already been demonstrated, the knowledge of the material properties necessary for such device optimization and real-life usage is very limited. In particular, carrier relaxation kinetics, relaxation pathways, and accompanied physical mechanisms, important for the laser's dynamics, have not been subjected to in-depth research and understanding. In this work, we present detailed spectroscopic studies on photoinjected carrier dynamics in $Ge_{1-x}Sn_x$ epilayers, as a function of Sn content (6−12%) and temperature (20−300 K), by utilizing time-resolved differential reflectivity and photoluminescence. The latter technique allowed us to track separated electron and hole dynamics with a femtosecond time resolution, while the former experiment exploited a joined electron−hole recombination. This experimental approach allowed us to identify (i) two initial electron relaxation processes after photoexcitation; (ii) radiative electron−hole recombination on below-band gap states; (iii) nonradiative carrier recombination involving the Shockley−Read−Hall mechanism; and (iv) nonradiative recombination through the surface states. The research results significantly expand the knowledge on the initial carrier relaxation dynamics in the $Ge_{1-x}Sn_x$ epitaxial material. It provides unknown up-to-date kinetic parameters of the initial stage of electron relaxation and further carrier recombination dynamics, unveils the critical role of band gap inhomogeneity for the relaxation dynamics, and highlights the role of below-band gap states that can participate in the light generation process in $Ge_{1-x}Sn_x$ epilayers.

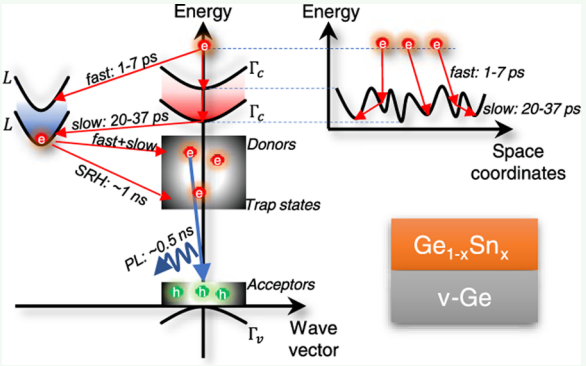

KEYWORDS: *Ge1−xSnx, carrier lifetime, carrier dynamics, electron relaxation, time-resolved photoluminescence, transient reflectivity, photoluminescence, photoreflectance*

1. INTRODUCTION

The development of silicon Si photonic devices operating in the mid-infrared (MIR) spectral region (3−50 μm) of electromagnetic spectrum has achieved remarkable progress.[1−3] Waveguides, splitters, resonators, modulators, switches, light detectors, and light sources are the key elements of the photonic integrated circuits that now can be merged into a single Si-based platform, achieving new functionalities and better performance at a reduced price and lower energy consumption. This should open vast application possibilities from free-space data communication[4] and MIR imaging of biological structures[5] to portable MIR lab-on-a-chip spectroscopic measurements[2] or tracing chemical elements in different states of matter using a sensor-in-a-chip platform.[2,6] Nevertheless, one of the major problems is a lack of the Si-compatible light source operating in the mid-infrared spectral region. Currently considered solutions include III−V (GaSb,[7,8] InP,[9,10] and others[11]) and group-IV ($Ge_{1-x}Sn_x$) semiconductor materials epitaxially grown directly on Si or via a relaxed Ge buffer.[12−15] The latter one, employing the $Ge_{1-x}Sn_x$ binary alloy, is a very attractive solution because it permits creation of all group-IV (Si, Ge, $Si_{1-x}Ge_x$, and $Ge_{1-x}Sn_x$) monolithically integrated photonic platform on Si. Since the first demonstration of the $Ge_{1-x}Sn_x$ lasing[16] at low temperature in 2015, the number of reports on the lasing in the bulk-like $Ge_{1-x}Sn_x$ material[17−25] has been expanding rapidly, giving a spark for further development of this technology.

Unstrained or bulk Ge is an indirect-gap semiconductor with a band gap energy of $E^{u}_{L,Ge} \approx 0.66$ eV at room temperature (RT) between the conduction band minimum at the L-point of the Brillouin zone and the valence band maximum at the Γ-point. The direct energy gap is shifted up ∼0.14 eV and

Received: October 6, 2020
Accepted: December 27, 2020
Published: January 11, 2021

https://dx.doi.org/10.1021/acsaelm.0c00889
ACS Appl. Electron. Mater. 2021, 3, 344−352

located at the Γ-point. Incorporation of Sn and formation of the $Ge_{1-x}Sn_x$ alloy cause faster energy downshift of the Γ-point conduction band minimum with the Sn content than that for the L-point.[26−30] It results in the conversion from the indirect to, favorable for optical devices, direct gap semiconductor at $x \sim 0.08$ and yields the direct energy gap tuning range between 0.6 eV (2.066 μm) and 0.29 eV (4.275 μm) at RT with the x varied from 0.08 to 0.23.[30−32] This picture can be strongly modified by the existence of strain originating from the ∼15% lattice mismatch between α-Sn and Ge, which shifts the indirect-to-direct band crossover to the higher Sn content.[33,34] Additionally, the strain relaxation at the higher Sn content may induce a large density of misfit dislocations, for example, edge and threading dislocations, stacking faults, and twin boundaries[35] that can strongly imprint radiative and nonradiative processes in $Ge_{1-x}Sn_x$, affecting the device performance. One would expect that this can as well imprint carrier relaxation dynamics important for dynamic parameters of devices.

Carrier relaxation dynamics in $Ge_{1-x}Sn_x$ epitaxial layers have not been studied in depth, mostly because of a problematic spectral range for the most suitable time-resolved experiments to be performed. The initial information comes from ref 16. Kinetic parameters were extracted not from time-resolved studies but indirectly evaluated from temperature-dependent PL experiments after applying a many-parameter physical model. In this case, the low-temperature (T = 10 K) carrier lifetime was estimated to ∼2.1 ns and decreased to ∼0.35 ns at RT following the temperature-dependent Shockley−Read−Hall (SRH) recombination process. Kinetic parameters were revealed only for a single, more than 200 nm-thick $Ge_{1-x}Sn_x$ layer. Later, in ref 36, the time-resolved photoluminescence (TRPL) technique was applied to measure T-dependent PL dynamics for a thin $Ge_{0.95}Sn_{0.05}$ layer. Data analysis yielded the carrier lifetime of ∼2.0 ns at T = 10 K, decreasing with temperature to ∼0.8 ns at T ≈ 150 K.[36] Furthermore, in this case, the SRH recombination processes were suggested as dominating the observed PL dynamics. Finally, a very recent study[37] utilized time-gated PL via the upconversion process in a nonlinear crystal and at T = 20 K revealed ∼217 ps carrier lifetime for a 350 nm-thick $Ge_{0.875}Sn_{0.125}$ layer, arguing that the SRH recombination is nearly temperature-independent, which is a striking difference to the conclusions derived from the previous research. The common drawback of the mentioned experiments is that the interpretation of experimental data comes from the PL, assuming to be originated from the direct-gap transition in $Ge_{1-x}Sn_x$ at a high enough Sn content. However, it is already proved that the PL can have its origin in point and extended defects at dislocations energetically located in the $Ge_{1-x}Sn_x$ band gap.[38] Therefore, the interpretation of carrier relaxation processes in $Ge_{1-x}Sn_x$ is an issue demanding more advanced research. This work aims to expand the knowledge on minority carrier dynamics in $Ge_{1-x}Sn_x$ epilayers with a variable Sn content ranging from 6 to 12%. The research is based on the complementary experimental techniques, PL, TRPL, photoreflectance ($\Delta R/R$), and time-resolved differential reflectivity (TRDR), revealing emission and absorption properties of the system in question and giving insights into radiative and nonradiative relaxation and recombination pathways. Based on both experiments' nature, we identify the separated contribution of defect-related radiative and trap-related nonradiative states to the overall carrier kinetics evolving differently in the temperature range between 10 and 300 K.

2. RESULTS AND DISCUSSION

2.1. Low-Temperature PL and Photoreflectance Experiments. The results of low-temperature PL and $\Delta R/R$ experiments presented in Figure 1 give a relevant background

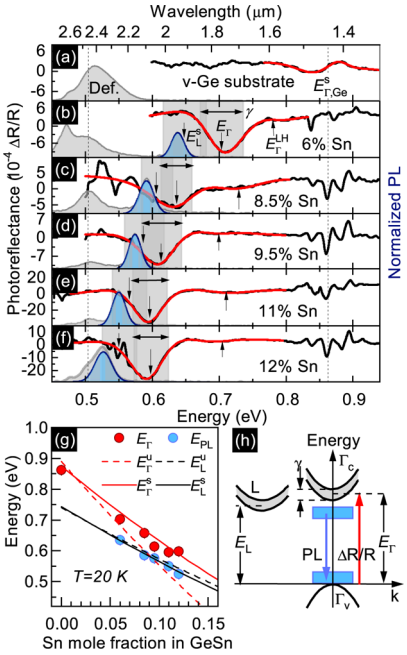

Figure 1. (a) $\Delta R/R$ (solid black line) and PL spectra (a shaded gray area) for the virtual Ge substrate (v-Ge) on Si. A solid red line indicates the fitting function as described in the Supporting Information, S2. (b−f) $\Delta R/R$ (solid black line) and PL spectra (a shaded gray area) for $Ge_{1-x}Sn_x$/v-Ge structures with various Sn contents. A Gaussian fit to the high-energy side PL peak is plotted in blue. A solid red line depicts the fits to the $Ge_{1-x}Sn_x$-related $\Delta R/R$ feature. The obtained direct energy gap ($E_\Gamma = E^{HH}_\Gamma$) is indicated by an arrow and so are the estimated indirect energy gap for the strained material (E^s_L) and the light-hole energy transition (E^{LH}_Γ). γ is a spectral broadening of the $\Delta R/R$ feature. T = 20 K, P_{PL} = 100 mW, d_{spot} = 150 μm. (g) E_Γ (red points) and PL peak energies (blue points) plotted with the Sn content in $Ge_{1-x}Sn_x$ epilayers. (h) Sketch of a $Ge_{1-x}Sn_x$ band structure in the momentum (k)-vector space with inhomogeneously broadened conduction bands (Γ_c and L). Γ_v is the valence band. Blue areas indicate below-band gap states for electrons and holes.

prior to discussing carrier dynamics in the $Ge_{1-x}Sn_x$ epilayers. Figure 1b−f (solid black line) presents $\Delta R/R$ features spread around 0.87 eV. These optical transitions are devoted to the absorption process involving the edges of valence and conduction bands at the Γ point of the Brillouin zone in germanium. It is confirmed by a similar type of $\Delta R/R$ feature shown in Figure 1a for the reference v-Ge substrate. In this case, the $\Delta R/R$ line shape was fitted to the low-field electromodulation formula (see the Supporting Information, S2). The extracted direct gap energy for the v-Ge epilayer is $E^s_{\Gamma,Ge}$ = 0.87 ± 0.02 eV, informing on the existence of residual strain. Raman spectroscopy (see the Supporting Information, S1) revealed that the built-in residual biaxial tensile strain is ∼0.23%, originating from the mismatch of the thermal

https://dx.doi.org/10.1021/acsaelm.0c00889
ACS Appl. Electron. Mater. 2021, 3, 344−352

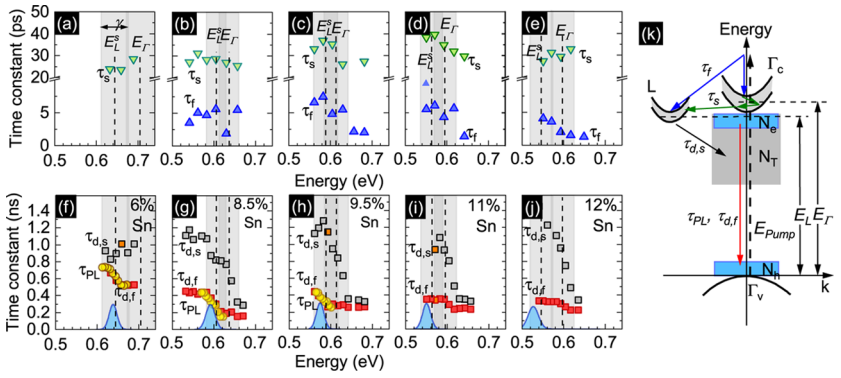

Figure 2. Energy dispersion of extracted kinetic parameters for $Ge_{1-x}Sn_x$ epilayers at T = 20 K and P_{pump} = 7 mW: (f–j) PL lifetime—τ_{PL} (yellow circles), short TRDR lifetime component—$\tau_{DR,s}$ (red squares), long TRDR lifetime component—$\tau_{DR,l}$ (open black squares). (a–e) Fast TRDR rise time component—τ_f (blue triangles), slow TRDR rise time component—τ_s (green triangles). Vertical dashed lines are the E_Γ energy. (k) Sketch of the $Ge_{1-x}Sn_x$ band structure with possible relaxation pathways indicated by solid arrows.

expansions between v-Ge and Si. The same conclusion holds for the v-Ge substrates with $Ge_{1-x}Sn_x$ epilayers on top.

Figure 1b–f reveals other $\Delta R/R$ features on the low-energy part of absorption-like spectra shifting toward lower energy with the increase in the Sn mole fraction. They are attributed to the absorption-like direct-gap optical transitions involving top-most, strain-split heavy-hole (HH) valence (Γ_v^{HH}) and conduction (Γ_c) bands at the Γ point of the Brillouin zone in $Ge_{1-x}Sn_x$ epilayers. The transition is sketched in Figure 1h as an up-pointed red arrow. The role of the strain-split light-hole (LH) valence band in optical transitions is omitted because of the sizable HH-LH splitting energy (>75 meV) and low oscillator strength of the Γ_v^{LH}–Γ_c optical transition (see the Supporting Information, S2). The effective direct gap energy (E_Γ) is extracted from $\Delta R/R$ features according to the fitting procedure described in the Supporting Information, S2. The fitting curves are plotted in Figure 1b–f (solid red line), with arrows indicating E_Γ^{HH} and E_Γ^{LH} energies. In the article, we refer to E_Γ^{HH} as E_Γ, if not otherwise stated. Please note that the $\Delta R/R$ features representing the direct gap optical transition in $Ge_{1-x}Sn_x$ are spectrally broad. The extracted broadening parameter (γ) equals around 50 meV for all the structures (see the Supporting Information, S2). It reflects the band gap inhomogeneity due to strain variation, electric field conditions, and fluctuation of chemical composition across the surface area from which the optical signal was derived. It is justified to assume that the spatial inhomogeneity of the Γ band is translated onto the L band and any other bands in $Ge_{1-x}Sn_x$ with significant consequences for the observed carrier dynamics. The spectral overlapping of the inhomogeneously broadened bands indicated in Figure 1b–f (superimposed gray-shaded rectangle areas centerd at the E_Γ and E_L^s) may suggest the multicomponent character of the time-resolved optical response taken from a different spectral region.

The extracted E_Γ plotted as a function of the Sn content in Figure 1g provides further information on the band structure of $Ge_{1-x}Sn_x$ epilayers. The figure contains calculated curves representing theoretically estimated changes in the direct and indirect-gap energy for the case of unstrained and compressively strained $Ge_{1-x}Sn_x$ materials (see the Supporting Information, S3). The comparison of E_Γ and theoretical values demonstrates that the examined epilayers are truly strained (see also the Supporting Information, S1, S2, and S5). The expected crossover between the indirect- and direct-gap $Ge_{1-x}Sn_x$ should occur at x > 0.20. It means that in the considered range of chemical composition, the $Ge_{1-x}Sn_x$ epilayers remain as indirect-gap semiconductors with poor abilities for light emission. However, this conclusion stays in contrast to the results of PL experiments presented in Figure 1b–f (gray- and blue-shaded areas).

The PL response consists of two superimposed emission bands. The lower energy PL band located near 0.51 eV is unchanging with the Sn mole fraction and matches PL emission from the reference v-Ge substrate presented in Figure 1a. This PL band is attributed to the electron–hole recombination at a defect on dislocation in germanium.[39,40] The higher energy PL band was fitted by a Gaussian-line profile plotted as a blue-shaded area in Figure 1b–f. The extracted PL peak energies (E_{PL}) are presented in Figure 1g (blue points), showing that the E_{PL} is shifting with the Sn mole fraction toward low energies. The observation suggests that the PL band is originated from a $Ge_{1-x}Sn_x$ epilayer. Moreover, the E_{PL} shows a sizable >39 meV downshift in respect to E_Γ (see the Supporting Information, Table S1), and apparently, it is lower than a theoretically estimated indirect energy gap (E_L^s) for the compressively strained $Ge_{1-x}Sn_x$. These findings suggest that the considered PL emission can have similar nature as the one observed for v-Ge at ∼0.51 eV. It can come from the electron–hole recombination at optically active defects on dislocations driven by the plastic strain relaxation in the $Ge_{1-x}Sn_x$ epilayers grown on the v-Ge substrate.[38,41,42] The defects are associated with the Lomer 90°[38]- or 60°[42]-type dislocations. In the latter case, it would form a band-like distribution of electronic states even up to ∼150 meV below the Γ_v. Other reports suggest the existence of point-like dislocation-related defects;[43] they may also be optically active. These defects are found 20–30 meV below the Γ_v.[43] They are partially energetically superimposed with the Sn-related acceptor-type multivacancy complexes spanning the range of 5–20 meV below the Γ_v.[43−45] These types of Sn-related shallow acceptors are speculated to be responsible for the p-type of unintentionally doped $Ge_{1-x}Sn_x$ epilayers.[44] These states are sketched as N_h in Figure 1h. Assuming the presence of donor states near the conduction band and depicting them as N_e in Figure 1h, the PL can be plotted as the optical transition between the N_e and N_h (downpointed blue arrow).

The conclusions from steady-state experiments are as follows: (i) the examined $Ge_{1-x}Sn_x$ epilayers are indirect-gap semiconductors with the lack of PL emission from the direct gap; (ii) PL emission comes from the below-band gap states;

https://dx.doi.org/10.1021/acsaelm.0c00889
ACS Appl. Electron. Mater. 2021, 3, 344–352

and (iii) the $Ge_{1-x}Sn_x$ band gap structure suffers spatial variations across the surface area of a sample indicated by the substantial ($\gamma > 39$ meV) broadening of the $\Delta R/R$ feature.

2.2. Low-Temperature TRDR and TRPL Experiments. The discussion on carrier dynamics in the $Ge_{1-x}Sn_x$ epilayers begins with presenting the results of the TRDR experiment at $T = 20$ K. The TRDR traces are recorded as a function of the probe pulse energy (E_{probe}) with a fixed pump pulse energy ($E_{pump} = 1.49$ eV) (see the Supporting Information, S4). The analysis yielded that the ascendant amplitude of TRDR is contributed by two processes having different time scales. The fitting procedure to the double exponential rise function provides two characteristic time constants nearly independent of the Sn mole fraction and E_{probe}: the fast one (τ_f) falling into the range of 1−7 ps and the slow one (τ_s) being within the 23−40 ps range. These results are summarized in Figure 2a−e. The lack of τ_f for the $Ge_{0.94}Sn_{0.06}$ epilayer is due to the small amplitude of an underlying process that could not be trustfully recovered by the fit. Because the structures are p-type, one can assume that relaxation mechanisms and possible relaxation pathways, which are behind the extracted kinetic parameters, are related to photogenerated minority carriers, namely, electrons.

In the beginning, we consider the building up of the carrier population at the states addressed by the E_{probe} above the effective E_Γ ($E_{probe} > E_\Gamma$), where the overlap of Γ_c and L bands is negligible. The electron population photoinjected much above the minimum of the Γ_c band is rapidly thermalizing to the bottom of the Γ_c band and to the X-band and finally to the L-band, through the interaction with optical and acoustic phonons. This is sketched by blue arrows in Figure 2k. The discussion skips Auger processes because of the insufficient photoinjected carrier population density, roughly 9×10^{13} cm^{-2} per pulse. For the reference case of germanium, the measured electron relaxation at $T = 300$ K is varied from 0.1−4 ps and includes electron relaxation within the Γ_c band (~0.1 ps),[46] hot electron transfer from Γ_c to L (0.2−0.4 ps),[46−50] cold electron transfer from Γ_c to L (1.2 ps),[51] X to L transition (0.4 ps),[50] and Γ_c to X transfer (0.1 ps).[52] At low temperatures, these time constants are expected to be slightly higher because of the lower phonon state density, and thus, relaxation times end up in a few ps range. One can conclude that the τ_f component extracted here for the $Ge_{1-x}Sn_x$ epilayers can have the same origin as mentioned above for germanium.

The existence of the τ_s component of the ascending TRDR amplitude at $E_{probe} > E_\Gamma$ is more puzzling. Although the carrier relaxation process among 3D densities of states to the bottom of the Γ_c should be relatively fast, as indicated by τ_f, it is hard to find other processes that could slow down the relaxation. However, we can propose the mechanism that emerges from the observed spatial inhomogeneity of the $Ge_{1-x}Sn_x$ band structure represented by the γ parameter. During the relaxation, carriers can be trapped by local confining potential islands spatially distributed within the spot area of an excitation pulse. Thus, the τ_s can represent carrier redistribution or a tunneling process between these confining potentials, similar to the carrier relaxation among spatially localized states in the 2D wetting layer of Stranski−Krastanow quantum dots.[53] This scenario seems to be supported by the temperature-dependent TRDR experiment that will be later discussed in the article.

For the case, when $E_L^s \le E_{probe} \le E_\Gamma$, the τ_f and τ_s are nearly unchanged as compared to the case when $E_{probe} > E_\Gamma$, which is nothing unexpected. A surprising finding is the lack of changes when the E_{probe} is below the L bands' spectrally broad distribution (see Figure 2b). It can suggest that fast building up of the carrier population at the bands' edges is equally efficient for some below band gap states, or the inhomogeneity of L bands is more extensive.

Let us move to discuss the slowly decaying TRDR amplitude, which is related to the depopulation of a density of states addressed by the E_{probe}. The TRDR decay curve analysis implies that at least two decay components contribute to it (see the Supporting Information, S4). Therefore, the decay is characterized by the fast ($\tau_{d,f}$) and slow ($\tau_{d,s}$) decay time constants plotted in Figure 2f−j as a function of E_{probe}.

First, we discuss the results when $E_{probe} < E_L^s$. Please note the spectral overlapping of the PL band (blue-shaded Gaussian profile) with the spectrally broadened E_L^s (gray-shaded rectangle) presented in Figure 2f−j. In this spectral range, the probe pulse measures a carrier population decay in at least two families of states: (a) below-band gap states associated with defects in $Ge_{1-x}Sn_x$ and partially contributing to the observed PL emission and (b) the L band states due to the band structure inhomogeneity. The extracted $\tau_{d,f}$ and $\tau_{d,s}$ are shifted apart, pointing to two different carrier relaxation pathways present in all the structures. For the $E_{probe} < E_L^s$, the $\tau_{d,s}$ is saturated at a maximum value without exhibiting a clear dispersion across the energy scale, reaching 0.9 ± 0.1 ns for the $Ge_{0.94}Sn_{0.06}$ epilayer and 1.1 ± 0.1 ns for the rest of the structures. Conversely, the $\tau_{d,s}$ shows a strong dispersion ($\tau_{d,f}(E_{probe})$) in the discussed energy range. For the $Ge_{0.94}Sn_{0.06}$ epilayer, the $\tau_{d,f}(E_{probe})$ increases from ~520 ps at $E_{probe} \approx E_\Gamma$ to ~730 ps at $E_{probe} < E_\Gamma$, defining the $\tau_{d,f}(E_{probe})$ variation range: $\Delta\tau_{d,f} \approx 210$ ps. When the Sn content increases, the high-energy value of $\tau_{d,f}(E_{probe})$ decreases accompanied by the decrease in $\Delta\tau_{d,f}$.

It is instructive to compare the results of TRDR with those from the TRPL experiment to identify the relaxation processes that stay behind the $\tau_{d,f}$ and $\tau_{d,s}$ kinetic parameters. These cases are limited to the $Ge_{1-x}Sn_x$ epilayers with $x = 0.06$, 0.085, and 0.095, for which the PL emission band is within the spectral range of the superconducting detector. The TRPL traces are recorded as a function of emission energy. Each TRPL trace is characterized by a resolution-limited rise and a slow, monoexponential decay (see the Supporting Information, S4). The extracted PL decay time (τ_{PL}) is plotted in Figure 2f−h (yellow points) as a function of emission energy. The $\tau_{PL}(E)$, which clearly starts below the E_L^s edge, is nearly identical to the $\tau_{d,f}(E_{probe})$. This observation allows ascribing the $\tau_{d,f}$ measured for the $E_{probe} < E_\Gamma$ as contributed by the effective radiative lifetime of electron−hole pairs at a defect band in $Ge_{1-x}Sn_x$, whereas the $\tau_{d,s}$ is attributed to the purely nonradiative recombination of presumable electrons in the L band within the trap states N_T, which are contributed either by the bulk traps or surface states. The energy dispersion of τ_{PL} and $\tau_{d,f}$ reminds the dispersion for optically active localized states in disordered semiconductor alloys[54,55] or quantum wells,[56,57] which could also be the case for the examined $Ge_{1-x}Sn_x$ epilayers. From this standpoint, the dispersion can be considered as generated by a carrier migration among optically active higher to lower energy states additionally affected by the nonradiative recombination channels.[54,55] The nonradiative recombination impact is reflected in the damping of the dispersion curve seen through the $\Delta\tau_{d,f}$ parameter. The $\Delta\tau_{d,f}$ steadily decreases with the increase in Sn content, from ~294 ps for the $Ge_{0.915}Sn_{0.085}$ to ~109 ps for the $Ge_{0.88}Sn_{0.012}$

https://dx.doi.org/10.1021/acsaelm.0c00889
ACS Appl. Electron. Mater. 2021, 3, 344−352

epilayer, and would be correlated with the increased number of nonradiative states generated by strain or point defects, which are induced by the incorporation of Sn atoms into the Ge matrix. Although the possible nature of radiative states has already been discussed for the steady-state experiments, it is hard to point to the specific nonradiative recombination centers. However, the $\tau_{d,s}$ measured in the energy range around the E_L^s edge can be tentatively assigned to the SRH recombination lifetime.

It is interesting to compare the TRPL results with those previously published. The ~2 ns PL lifetime reported in ref 36 for a thin $Ge_{0.95}Sn_{0.05}$ layer is longer than ~0.5 ns obtained here. On one hand, it could be related to a high-excitation condition specific for the performed experiment. On the other hand, the reported epilayer could have good optical quality, translating to reduced nonradiative recombination. The results presented in ref 37 seem to be more consistent with ours. The ~217 ps PL lifetime for the 350 nm-thick $Ge_{0.875}Sn_{0.125}$ is comparable to ~320 ps for the 36 nm-thick $Ge_{0.88}Sn_{0.12}$ epilayer. The lifetime difference can be attributed to the thick epilayer's deteriorated crystal quality due to a bit higher Sn content and strain relaxation[35] above the critical thickness leading to the enlargement of defect state density. Note that literature data did not provide any other kinetic parameters related to nonradiative recombination channels.

Now, we shift the discussion toward $\tau_{d,f}$ and $\tau_{d,s}$ obtained at energy states above the $Ge_{1-x}Sn_x$ conduction band minimum ($E_{probe} > E_L^s$). In this case, Figure 2f–j shows that the $\tau_{d,s}$ is relatively little affected when the E_{probe} approaches the E_L^s, but it suffers a huge drop when crossing the E_Γ. To interpret this observation, one needs to recall the substantial inhomogeneity of the L and Γ bands resulting in a spectral overlap of related densities of states. Thus, for $E_{probe} > E_\Gamma$, the contribution of rapid relaxation phenomena represented by τ_f and τ_s overcomes the nonradiative relaxation that occurs on the decreasing number of states at the high-energy tail of the L-band distribution. Conversely, when the E_{probe} approaches the low-energy tail of the inhomogeneously broadened L band distribution, the rapid relaxation processes' contribution is reduced. Thus, the $\tau_{d,s}$ is governed by a relatively slow nonradiative relaxation at the L-band. It is also affected by the carrier relaxation at the high-energy tail of the defect distribution.

The more puzzling behavior concerns the $\tau_{d,f}$. As it was already stated, for $E_{probe} < E_L^s$, the $\tau_{d,f}$ is partially related to radiative recombination at below-band gap states and suffers the characteristic energy dispersion. However, when the E_{probe} is shifting above the E_L^s, the $\tau_{d,f}(E_{probe})$ is getting nearly dispersionless even above the effective E_Γ. The $\tau_{d,f} \approx 200$ ps obtained for the structures at $E_{probe} > E_L^s$ is close to the value of surface recombination lifetime (~500 ps) estimated from the $\tau_{surf} = W/2s$ expression.[58] Here, the surface recombination velocity $s = 4000$ cm s^{-1} obtained for the Ge/Si interface[59] and the layer thickness W are taken from Table 1. A similar surface recombination velocity of 170 ± 35 ps was measured for the 220 nm-thick $Ge_{0.875}Sn_{0.125}$ epilayer on Ge.[60] Therefore, we believe that $\tau_{d,f}$ is getting dominated by the surface recombination at the $Ge_{1-x}Sn_x$/Ge or $Ge_{1-x}Sn_x$/air interface.

2.3. Temperature-dependent TRDR and TRPL Experiments. The temperature-dependent TRDR experiment provides additional arguments supporting the stated hypothesis on existing carrier relaxation channels and mechanisms in the studied $Ge_{1-x}Sn_x$ epilayers. Three $Ge_{1-x}Sn_x$ epilayers were selected for these studies having the Sn content of 6, 9.5, and 11%. In the experiment, $E_{probe} \approx E_L^s$ (see orange points in Figure 2f,h,i) accounts for the temperature-driven $Ge_{1-x}Sn_x$ band gap evolution. The extracted TRDR amplitude rise ($\tau_f(T)$, $\tau_s(T)$) and decay times ($\tau_{d,f}(T)$, $\tau_{d,s}(T)$) from the TRDR traces are plotted in Figure 3. Figure 3a shows that both rise times are getting shorter with T. The overall decrease in the τ_f reaches a few picoseconds between low and high temperature, whereas the reduction in the τ_s is a few tens of picoseconds. The behavior of the $\tau_s(T)$ function can be interpreted with the postulated picture that includes spatial fluctuation of the $Ge_{1-x}Sn_x$ band gap. The decline of $\tau_d(T)$ with T can be governed by the smearing of spatially distributed inhomogeneous confining potentials by the k_BT energy, where k_B is the Boltzmann constant. Besides, the increasing phonon population at elevated temperatures accelerates carrier phonon scattering and increases energy relaxation and carrier transfer efficiency among localized sites. It leads to the diminishing of the role of spatial localization, promoting the fast carrier relaxation typical for the bulk material over the carrier hoping-like processes among localized sites in inhomogeneous $Ge_{1-x}Sn_x$.[61]

Table 1. Information on the $Ge_{1-x}Sn_x$ Epilayers[a] Studied Here

Sn content (%)	thickness (nm)	strain (%)
6.0	44	−0.62
8.5	63	−0.95
9.5	54	−1.08
11.0	48	−1.30
12.0	36	−1.48

[a]Chemical content is obtained from a high-resolution X-ray diffraction experiment, and the thickness is evaluated from cross-sectional transmission electron microscopy pictures of the structures. Strain values are obtained from the analysis of Raman spectroscopy data (see the Supporting Information, S1).

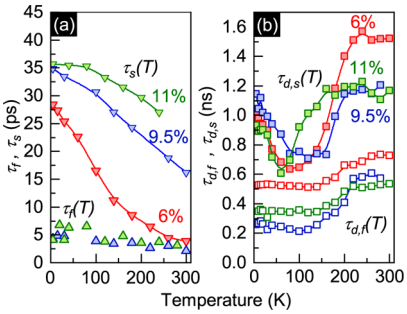

Figure 3. Temperature dependence of (a) TRDR rise times (τ_f, τ_s) and (b) TRDR decay times ($\tau_{d,f}$, $\tau_{d,s}$) extracted for the $Ge_{1-x}Sn_x$ epilayers with $x = 0.06$ (open and full triangles and squares in red), $x = 0.095$ (open and full triangles and squares in green), $x = 0.11$ (open and full triangles and squares in blue). Red, green, and blue lines in (a) represent the fitting curves for a phonon-mediated relaxation process. Red, green, and blue dashed lines in (b) are guides to the eye. $E_{pump} = 1.52$ eV, $E_{probe} \approx E_\Gamma$, and $P_{pump} = 7$ mW.

The temperature evolution of decay time constants presented in Figure 3b shows that the observed carrier recombination channels identified by $\tau_{d,s}$ and $\tau_{d,f}$ have a different origin because of the very different temperature characteristics. In the temperature range 10–100 K, the $\tau_{d,s}(T)$ decreases almost twice with T. This behavior is consistent with

https://dx.doi.org/10.1021/acsaelm.0c00889
ACS Appl. Electron. Mater. 2021, 3, 344–352

the bulk-like SRH process. The carrier capture efficiency by trap states N_T increases with temperature.[58] Interestingly, the speedup of nonradiative recombination is accompanied by the T-enhanced carrier population at the examined states reflected in the increase in $\tau_{d,s}(T)$ for $T > 100$ K. The activation temperature at which the states located near the E_L^s are getting populated varies from ∼80 K for the $Ge_{0.89}Sn_{0.11}$ epilayer to ∼160 K for the $Ge_{0.905}Sn_{0.095}$ and $Ge_{0.94}Sn_{0.06}$ epilayers. The smallest activation temperature for the highest-Sn content structure can be attributed to the larger population of trap states with their wider energy distribution in the $Ge_{1-x}Sn_x$ band gap. It is interesting to correlate this specific $\tau_{d,s}(T)$ function with the published results of electrical measurements performed on $Ge_{1-x}Sn_x$, looking for a possible origin for the carrier activation source at elevated temperatures. Conley et al.[45] have investigated temperature-dependent electrical transport characteristics extracted from the dark current−voltage curves of a $Ge_{1-x}Sn_x$/Ge device. The dark resistance of a device stops decreasing at T ≈ 160 K with increasing temperature, attributed to the increasing number of carriers in the conduction band originated from the unspecified surface or bulk-like defect states. Takeuchi et al.[43] have used conventional deep-level transient spectroscopy (DLTS) to study defects in a $Ge_{1-x}Sn_x$/Ge diode. The temperature-controlled DLTS experiment allowed us to identify minority carrier (electrons) traps in the diode showing pronounced DLTS deeps at ∼100 and ∼150 K. These were attributed to defects at the heterojunction and the bulk-like-traps in the $Ge_{1-x}Sn_x$ epilayer and/or the virtual Ge substrate, respectively. However, the exact origin of defects was not clarified. Finally, in ref 42 the DLTS experiment has also been used to investigate the $Ge_{1-x}Sn_x$/Ge junction diode. The DLTS spectra have revealed deeps smeared between 100 and 150 K. The deeps were attributed to the extended defect-like states identified as the deep, repulsive-like donor centers with a band-like distribution in the $Ge_{1-x}Sn_x$ band gap. In the same studies, the T-dependent reverse-bias current density increased significantly at $T > 160$ K, suggesting that these defects may be a source of minority carriers in the conduction band at elevated temperatures.

The abovementioned temperature-driven carrier dynamics can be completed by the discussion on the $\tau_{d,f}(T)$ function. Figure 3b shows that the $\tau_{d,f}(T)$ is nearly temperature-independent up to $T \approx 150$ K, which is in high contrast to the $\tau_{d,s}(T)$ function. At $T > 150$ K, the $\tau_{d,f}$ slightly increases with T but not as much as the $\tau_{d,s}$. Although the SRH recombination involves the deep, bulk-like traps, the $\tau_{d,f}$ obtained at E_L^s must describe another recombination channel. Because it is weakly temperature-dependent, it could be indeed related to the surface recombination.

3. CONCLUSIONS

In conclusion, we investigated carrier dynamics in compressively strained and indirect-band gap $Ge_{1-x}Sn_x$ epilayers grown on a Ge/Si(001) virtual substrate. Sn content, x, was varied between 6 and 12%. The use of complementary optical methods, including TRDR and TRPL, supported by data obtained from the steady-state spectroscopic experiments (PL, $\Delta R/R$, and Raman) allowed us to measure carrier kinetics and to identify possible carrier relaxation pathways and recombination mechanisms. Our results show some similarities to previous reports on carrier dynamics in $Ge_{1-x}Sn_x$ epilayers, but they considerably expand knowledge on newly observed carrier recombination channels, unveiled by the TRDR experiment.

We found that initial electron relaxation just after the photoexcitation at $T = 20$ K is contributed by two processes: fast one characterized by the 1−7 ps relaxation time and slow one falling into the range of 23−40 ps. This was not previously reported for $Ge_{1-x}Sn_x$ epilayers. The fast relaxation process is related to electron thermalization through interactions of phonons to the bottom of the Γ band and further to the L band, whereas the slower process is attributed to the postulated carrier transfer between spatially localized potential landscapes generated by the inherent inhomogeneities of $Ge_{1-x}Sn_x$ epilayers. Thermal averaging of confining potentials with increasing temperature leads to a substantial speedup of the slow component toward the values of the fast relaxation time. The initial electron relaxation is followed by its radiative and nonradiative recombination reflected in the composite optical response. Because the band gap in the researched $Ge_{1-x}Sn_x$ epilayers is indirect, the observed PL process is related to the electron−hole recombination at below-band gap localized states, in vicinity of the nonradiative recombination. The strong dispersion of PL lifetime across the PL energy band suggests carrier transfer within optically active below-band gap states. The nonradiative recombination at the mobility edge of $Ge_{1-x}Sn_x$ epilayers is due to two processes: the SRH one identified by its strong temperature dependence and the surface recombination process that is almost temperature-independent. The low-temperature SRH lifetime is nearly 1 ns, while the surface recombination time is close to 200 ps with negligible dependence on Sn content in the $Ge_{1-x}Sn_x$ epilayers.

These findings allow us to obtain a perspective on $Ge_{1-x}Sn_x$-based applications. On one side, the rapid intraband relaxation time, up to a few ps, is plausible for a high modulation speed of a laser and an optical amplifier, quick changes of a device's state in the case of optical switches, and a fast response time of a photodetector. On another side, the apparently high efficiency of nonradiative processes observed in the investigated $Ge_{1-x}Sn_x$ epilayers can be unfavorable for optoelectronic devices. In $Ge_{1-x}Sn_x$-based photodetectors, the relevant time scale heavily relies on rapid intraband relaxation, which is at least 2 orders of magnitude faster than surface recombination time and bulk-like SRH processes. Moreover, a thin $Ge_{1-x}Sn_x$ layer in a photodetector is plausible, providing an efficient charge separation length. Additional surface passivation can diminish the effect of strong surface recombination, increasing the overall performance of the device by decreasing the dark current density.

Also, the fast surface recombination is vital for electrically driven light-emitting devices because the carrier losses upon injection increase the threshold current density. In this case, equally important is the SRH recombination. Omitting the discussion on the nature of lasing states in the $Ge_{1-x}Sn_x$ epilayers, we can extrapolate our results on typically used thick $Ge_{1-x}Sn_x$ layers in laser devices. We believe that increasing the thickness of a $Ge_{1-x}Sn_x$ epilayer above the critical thickness results in a strain relaxation. This process introduces defects at the interface strained relaxed $Ge_{1-x}Sn_x$ and Ge epilayers and within the $Ge_{1-x}Sn_x$ epilayer. These defects act as efficient nonradiative recombination centers. Thus, in thick $Ge_{1-x}Sn_x$ epilayers, the SRH processes are expected to play a more significant role than that reported in our work. However, lasing is still possible at the cost of high injection current density, which is a major disadvantage.

https://dx.doi.org/10.1021/acsaelm.0c00889
ACS Appl. Electron. Mater. 2021, 3, 344−352

Finally, we can speculate on a possible origin of the density of states, taking part in a lasing process. We have already underlined an essential role of electronic states located within the $Ge_{1-x}Sn_x$ band gap acting as efficient radiative recombination centers despite the indirect-band character of researched $Ge_{1-x}Sn_x$ epilayers. These states can play a major role in the lasing process. However, there is another scenario that could be realized in $Ge_{1-x}Sn_x$ epilayers. Because the electron lifetime on the trap states and defects on dislocations remains quite long, under a high carrier injection regime, which is typical for laser operation, the carrier relaxation to these states is appearing to be inefficient. Thus, the remaining high density of photoinjected carriers in the mobility edge of $Ge_{1-x}Sn_x$ could be responsible for the lasing process.

4. METHODS

4.1. $Ge_{1-x}Sn_x$ Sample Growth. Epitaxial materials for this research were grown with the help of chemical vapor deposition at reduced pressure in an industrial-type ASM Epsilon 2000 system and on 200 mm-diameter Si(001) wafers. The epitaxial structure consists of a ∼700 nm-thick relaxed Ge buffer followed by a compressively strained $Ge_{1-x}Sn_x$ epilayer on the surface. Commercial and purified GeH_4 and $SnCl_4$ precursors were used to grow $Ge_{1-x}Sn_x$ epilayers. The epitaxial process was carried out in a hydrogen atmosphere at a reduced pressure. The epitaxial materials are intentionally undoped. Five structures with Sn contents of 6, 8.5, 9.5, 11, and 12% in the $Ge_{1-x}Sn_x$ epilayers were used in this research. In addition, the relaxed Ge buffer on Si was grown and used as a reference. The chemical composition and thickness of each epilayer are summarized in Table 1. The state of strain in each epilayer and Sn content in the $Ge_{1-x}Sn_x$ epilayer were measured by high-resolution X-ray diffraction (HR-XRD) (see the Supporting Information, S5). Epilayers' thicknesses were obtained with the help of XTEM. More details about the sample growth and structural data can be found elsewhere.[32,36,38,62]

4.2. Steady-State Spectroscopic Measurements. Structures were enclosed in a helium-flow optical cryostat, allowing for the sample temperature control in the range of 10−300 K. In the absorption-like $\Delta R/R$ experiment, a halogen lamp was used as a broadband probe beam source. The 630 nm line from a semiconductor diode laser was employed for photomodulation purposes. The 0.3 m-focal length monochromator dispersed the white light reflected off the sample and measured via the lock-in technique at the reference modulation frequency of 280 Hz, using a thermoelectrically cooled PbS photodiode. The same experimental configuration with the switched-off halogen lamp was used for measuring the steady-state PL spectra.

4.3. Time-Resolved Differential Reflectivity Experiment. The experiment is set up in the reflection mode. A Ti:sapphire ultrafast oscillator was used as an excitation source.[61,63] The oscillator generates trains of ∼140 fs-long pump pulses at a repetition frequency of 76 MHz with the E_{pump} = 1.49 eV photon energy in the pulse. The pulse train synchronously feeds the optical parametric oscillator, in which the nonlinear photon energy conversion allowed for the tuning of the probe pulse photon energy in the range of ∼0.54 to ∼0.67 eV. The length of a probe pulse was ∼230 fs with the corresponding pulse broadening of ≈8 meV. The time delay between probe and pump pulses arriving at the sample surface was set by varying a mechanical delay line providing a resolution of ∼0.3 ps.

4.4. Time-Resolved Photoluminescence. TRPL was measured with a standard PL setup by a time-correlated single-photon counting method. In this case, a structure was excited at E_{exc} = 1.49 eV by a train of ∼140 fs-long pulses from the Ti:sapphire oscillator. The TRPL signal was filtered using a 0.5 m-long monochromator, and photons were collected using a NbN superconducting detector. The overall temporal resolution of the TRPL setup was ∼80 ps.[64]

■ ASSOCIATED CONTENT

Supporting Information

The Supporting Information is available free of charge at https://pubs.acs.org/doi/10.1021/acsaelm.0c00889.

Rogowicz et al. Raman spectroscopy of the v-Ge substrate and $Ge_{1-x}Sn_x$ epilayers; fitting parameters of $\Delta R/R$ features for the $Ge_{1-x}Sn_x$ epilayers; theoretical estimations of the $Ge_{1-x}Sn_x$ band structure evolution with the Sn mole fraction; examples of time-resolved differential reflectivity and TRPL traces; and example of XRD traces for the high-Sn content $Ge_{1-x}Sn_x$ epilayer (PDF)

■ AUTHOR INFORMATION

Corresponding Authors

Ernest Rogowicz − *Faculty of Fundamental Problems of Technology, Department of Experimental Physics, Wrocław University of Science and Technology, 50-370 Wrocław, Poland;* orcid.org/0000-0002-6441-9463; Email: ernest.rogowicz@pwr.edu.pl

Maksym Myronov − *Department of Physics, The University of Warwick, CV4 7AL Coventry, U.K.;* orcid.org/0000-0001-7757-2187; Email: m.myronov@warwick.ac.uk

Robert Kudrawiec − *Faculty of Fundamental Problems of Technology, Department of Semiconductor Materials Engineering, Wrocław University of Science and Technology, 50-370 Wrocław, Poland;* orcid.org/0000-0003-2593-9172; Email: robert.kudrawiec@pwr.edu.pl

Marcin Syperek − *Faculty of Fundamental Problems of Technology, Department of Experimental Physics, Wrocław University of Science and Technology, 50-370 Wrocław, Poland*; Email: marcin.syperek@pwr.edu.pl

Authors

Jan Kopaczek − *Faculty of Fundamental Problems of Technology, Department of Semiconductor Materials Engineering, Wrocław University of Science and Technology, 50-370 Wrocław, Poland*

Joanna Kutrowska-Girzycka − *Faculty of Fundamental Problems of Technology, Department of Experimental Physics, Wrocław University of Science and Technology, 50-370 Wrocław, Poland*

Complete contact information is available at: https://pubs.acs.org/10.1021/acsaelm.0c00889

Notes

The authors declare no competing financial interest.

■ ACKNOWLEDGMENTS

This work was supported by The Polish National Science Centre through grant no. 2016/21/B/ST7/01267. M.M. acknowledges the financial support from The Engineering and Physical Sciences Research Council (EPSRC).

■ REFERENCES

(1) Roelkens, G.; Dave, U.; Gassenq, A.; Hattasan, N.; Chen Hu, C.; Kuyken, B.; Leo, F.; Malik, A.; Muneeb, M.; Ryckeboer, E.; Sanchez, D.; Uvin, S.; Wang, R.; Hens, Z.; Baets, R.; Shimura, Y.; Gencarelli, F.; Vincent, B.; Loo, R.; Van Campenhout, J.; Cerutti, L.; Rodriguez, J.-B.; Tournie, E.; Xia Chen, X.; Nedeljkovic, M.; Mashanovich, G.; Li Shen, L.; Healy, N.; Peacock, A. C.; Xiaoping Liu, X.; Osgood, R.; Green, W. M. J. Silicon-Based Photonic Integration Beyond the

Telecommunication Wavelength Range. *IEEE J. Sel. Top. Quantum Electron.* **2014**, *20*, 394−404.
(2) Lin, H.; Luo, Z.; Gu, T.; Kimerling, L. C.; Wada, K.; Agarwal, A.; Hu, J. Mid-infrared integrated photonics on silicon: a perspective. *Nanophotonics* **2017**, *7*, 393−420.
(3) Fedeli, J.-M.; Nicoletti, S. Mid-Infrared (Mid-IR) Silicon-Based Photonics. *Proc. IEEE* **2018**, *106*, 2302−2312.
(4) Liu, J. J.; Stann, B. L.; Klett, K. K.; Cho, P. S.; Pellegrino, P. M. Mid and Long-Wave Infrared Free-Space Optical communication. *Laser Communication and Propagation through the Atmosphere and Oceans VIII*, 2019; pp 1−18.
(5) Hermes, M.; Morrish, R. B.; Huot, L.; Meng, L.; Junaid, S.; Tomko, J.; Lloyd, G. R.; Masselink, W. T.; Tidemand-Lichtenberg, P.; Pedersen, C.; Palombo, F.; Stone, N. Mid-IR hyperspectral imaging for label-free histopathology and cytology. *J. Opt.* **2018**, *20*, 023002.
(6) Haas, J.; Mizaikoff, B. Advances in Mid-Infrared Spectroscopy for Chemical Analysis. *Annu. Rev. Anal. Chem.* **2016**, *9*, 45−68.
(7) Hattasan, N.; Gassenq, A.; Cerutti, L.; Rodriguez, J. B.; Tournié, E.; Roelkens, G. GaSb-based integrated lasers and photodetectors on a Silicon-On-Insulator waveguide circuit for sensing applications in the shortwave infrared. *2012 Photonics Global Conference (PGC)*, 2012; pp 1−4.
(8) Wang, R.; Malik, A.; Šimonytė, I.; Vizbaras, A.; Vizbaras, K.; Roelkens, G. Compact GaSb/silicon-on-insulator 2.0 μm widely tunable external cavity lasers. *Opt. Express* **2016**, *24*, 28977.
(9) Spott, A.; Davenport, M.; Peters, J.; Bovington, J.; Heck, M. J. R.; Stanton, E. J.; Vurgaftman, I.; Meyer, J.; Bowers, J. Heterogeneously integrated 2.0 μm CW hybrid silicon lasers at room temperature. *Opt. Lett.* **2015**, *40*, 1480.
(10) Wang, R.; Sprengel, S.; Malik, A.; Vasiliev, A.; Boehm, G.; Baets, R.; Amann, M.-C.; Roelkens, G. Heterogeneously integrated III−V-on-silicon 2.3x μm distributed feedback lasers based on a type-II active region. *Appl. Phys. Lett.* **2016**, *109*, 221111.
(11) Spott, A.; Peters, J.; Davenport, M.; Stanton, E.; Zhang, C.; Merritt, C.; Bewley, W.; Vurgaftman, I.; Kim, C.; Meyer, J.; Kirch, J.; Mawst, L.; Botez, D.; Bowers, J. Heterogeneously Integrated Distributed Feedback Quantum Cascade Lasers on Silicon. *Photonics* **2016**, *3*, 35.
(12) Liu, X.; Osgood, R. M.; Vlasov, Y. A.; Green, W. M. J. Mid-infrared optical parametric amplifier using silicon nanophotonic waveguides. *Nat. Photonics* **2010**, *4*, 557−560.
(13) Lau, R. K. W.; Ménard, M.; Okawachi, Y.; Foster, M. A.; Turner-Foster, A. C.; Salem, R.; Lipson, M.; Gaeta, A. L. Continuous-wave mid-infrared frequency conversion in silicon nanowaveguides. *Opt. Lett.* **2011**, *36*, 1263.
(14) Kuyken, B.; Verheyen, P.; Tannouri, P.; Liu, X.; Van Campenhout, J.; Baets, R.; Green, W. M. J.; Roelkens, G. Generation of 3.6 μm radiation and telecom-band amplification by four-wave mixing in a silicon waveguide with normal group velocity dispersion. *Opt. Lett.* **2014**, *39*, 1349.
(15) Singh, N.; Hudson, D. D.; Yu, Y.; Grillet, C.; Jackson, S. D.; Casas-Bedoya, A.; Read, A.; Atanackovic, P.; Duvall, S. G.; Palomba, S.; Luther-Davies, B.; Madden, S.; Moss, D. J.; Eggleton, B. J. Midinfrared supercontinuum generation from 2 to 6 μm in a silicon nanowire. *Optica* **2015**, *2*, 797.
(16) Wirths, S.; Geiger, R.; von den Driesch, N.; Mussler, G.; Stoica, T.; Mantl, S.; Ikonic, Z.; Luysberg, M.; Chiussi, S.; Hartmann, J. M.; Sigg, H.; Faist, J.; Buca, D.; Grützmacher, D. Lasing in direct-bandgap GeSn alloy grown on Si. *Nat. Photonics* **2015**, *9*, 88−92.
(17) Al-Kabi, S.; Ghetmiri, S. A.; Margetis, J.; Pham, T.; Zhou, Y.; Dou, W.; Collier, B.; Quinde, R.; Du, W.; Mosleh, A.; Liu, J.; Sun, G.; Soref, R. A.; Tolle, J.; Li, B.; Mortazavi, M.; Naseem, H. A.; Yu, S.-Q. An optically pumped 2.5 μm GeSn laser on Si operating at 110 K. *Appl. Phys. Lett.* **2016**, *109*, 171105.
(18) Stange, D.; Wirths, S.; Geiger, R.; Schulte-Braucks, C.; Marzban, B.; von den Driesch, N.; Mussler, G.; Zabel, T.; Stoica, T.; Hartmann, J.-M.; Mantl, S.; Ikonic, Z.; Grützmacher, D.; Sigg, H.; Witzens, J.; Buca, D. Optically Pumped GeSn Microdisk Lasers on Si. *ACS Photonics* **2016**, *3*, 1279−1285.
(19) Margetis, J.; Al-Kabi, S.; Du, W.; Dou, W.; Zhou, Y.; Pham, T.; Grant, P.; Ghetmiri, S.; Mosleh, A.; Li, B.; Liu, J.; Sun, G.; Soref, R.; Tolle, J.; Mortazavi, M.; Yu, S.-Q. Si-Based GeSn Lasers with Wavelength Coverage of 2−3 μm and Operating Temperatures up to 180 K. *ACS Photonics* **2017**, *5*, 827−833.
(20) Reboud, V.; Gassenq, A.; Pauc, N.; Aubin, J.; Milord, L.; Thai, Q. M.; Bertrand, M.; Guilloy, K.; Rouchon, D.; Rothman, J.; Zabel, T.; Armand Pilon, F.; Sigg, H.; Chelnokov, A.; Hartmann, J. M.; Calvo, V. Optically pumped GeSn micro-disks with 16% Sn lasing at 3.1 μm up to 180 K. *Appl. Phys. Lett.* **2017**, *111*, 092101.
(21) Dou, W.; Zhou, Y.; Margetis, J.; Ghetmiri, S. A.; Al-Kabi, S.; Du, W.; Liu, J.; Sun, G.; Soref, R. A.; Tolle, J.; Li, B.; Mortazavi, M.; Yu, S.-Q. Optically pumped lasing at 3 μm from compositionally graded GeSn with tin up to 22.3 %. *Opt. Lett.* **2018**, *43*, 4558.
(22) Huang, B.-J.; Chang, C.-Y.; Hsieh, Y.-D.; Soref, R. A.; Sun, G.; Cheng, H.-H.; Chang, G.-E. Electrically Injected GeSn Vertical-Cavity Surface Emitters on Silicon-on-Insulator Platforms. *ACS Photonics* **2019**, *6*, 1931−1938.
(23) Zhou, Y.; Dou, W.; Du, W.; Ojo, S.; Tran, H.; Ghetmiri, S. A.; Liu, J.; Sun, G.; Soref, R.; Margetis, J.; Tolle, J.; Li, B.; Chen, Z.; Mortazavi, M.; Yu, S.-Q. Optically Pumped GeSn Lasers Operating at 270 K with Broad Waveguide Structures on Si. *ACS Photonics* **2019**, *6*, 1434−1441.
(24) Chrétien, J.; Pauc, N.; Armand Pilon, F.; Bertrand, M.; Thai, Q.-M.; Casiez, L.; Bernier, N.; Dansas, H.; Gergaud, P.; Delamadeleine, E.; Khazaka, R.; Sigg, H.; Faist, J.; Chelnokov, A.; Reboud, V.; Hartmann, J.-M.; Calvo, V. GeSn Lasers Covering a Wide Wavelength Range Thanks to Uniaxial Tensile Strain. *ACS Photonics* **2019**, *6*, 2462−2469.
(25) Elbaz, A.; Buca, D.; von den Driesch, N.; Pantzas, K.; Patriarche, G.; Zerounian, N.; Herth, E.; Checoury, X.; Sauvage, S.; Sagnes, I.; Foti, A.; Ossikovski, R.; Hartmann, J.-M.; Boeuf, F.; Ikonic, Z.; Boucaud, P.; Grützmacher, D.; El Kurdi, M. Ultra-low-threshold continuous-wave and pulsed lasing in tensile-strained GeSn alloys. *Nat. Photonics* **2020**, *14*, 375−382.
(26) He, G.; Atwater, H. A. Interband Transitions in Sn_xGe_{1-x} Alloys. *Phys. Rev. Lett.* **1997**, *79*, 1937−1940.
(27) D'Costa, V. R.; Cook, C. S.; Birdwell, A. G.; Littler, C. L.; Canonico, M.; Zollner, S.; Kouvetakis, J.; Menéndez, J. Optical critical points of thin-film $Ge_{1-y}Sn_y$ alloys: A comparative $Ge_{1-y}Sn_y/Ge_{1-x}Si_x$ study. *Phys. Rev. B* **2006**, *73*, 125207.
(28) Eckhardt, C.; Hummer, K.; Kresse, G. Indirect-to-direct gap transition in strained and unstrained Sn_xGe_{1-x} alloys. *Phys. Rev. B* **2014**, *89*, 165201.
(29) Yin, W.-J.; Gong, X.-G.; Wei, S.-H. Origin of the unusually large band-gap bowing and the breakdown of the band-edge distribution rule in the Sn_xGe_{1-x} alloys. *Phys. Rev. B* **2008**, *78*, 161203.
(30) Polak, M. P.; Scharoch, P.; Kudrawiec, R. The electronic band structure of $Ge_{1-x}Sn_x$ in the full composition range: indirect, direct, and inverted gaps regimes, band offsets, and the Burstein−Moss effect. *J. Phys. D: Appl. Phys.* **2017**, *50*, 195103.
(31) Zhu, Z.; Xiao, J.; Sun, H.; Hu, Y.; Cao, R.; Wang, Y.; Zhao, L.; Zhuang, J. Composition-dependent band gaps and indirect−direct band gap transitions of group-IV semiconductor alloys. *Phys. Chem. Chem. Phys.* **2015**, *17*, 21605−21610.
(32) Millar, R. W.; Dumas, D. C. S.; Gallacher, K. F.; Jahandar, P.; MacGregor, C.; Myronov, M.; Paul, D. J. Mid-infrared light emission > 3 μm wavelength from tensile strained GeSn microdisks. *Opt. Express* **2017**, *25*, 25374−25385.
(33) Dybała, F.; Żelazna, F.; Mączko, H.; Gładysiewicz, M.; Misiewicz, J.; Kudrawiec, R.; Lin, H.; Chen, R.; Shang, C.; Huo, Y.; Kamins, T. I.; Harris, J. S. Electromodulation spectroscopy of direct optical transitions in $Ge_{1-x}Sn_x$ layers under hydrostatic pressure and built-in strain. *J. Appl. Phys.* **2016**, *119*, 215703.
(34) Liu, Z.; Cong, H.; Yang, F.; Li, C.; Zheng, J.; Xue, C.; Zuo, Y.; Cheng, B.; Wang, Q. Defect-free high Sn-content GeSn on insulator grown by rapid melting growth. *Sci. Rep.* **2016**, *6*, 38386.
(35) Assali, S.; Elsayed, M.; Nicolas, J.; Liedke, M. O.; Wagner, A.; Butterling, M.; Krause-Rehberg, R.; Moutanabbir, O. Vacancy

https://dx.doi.org/10.1021/acsaelm.0c00889
ACS Appl. Electron. Mater. 2021, 3, 344−352

complexes in nonequilibrium germanium-tin semiconductors. *Appl. Phys. Lett.* **2019**, *114*, 251907.
(36) De Cesari, S.; Balocchi, A.; Vitiello, E.; Jahandar, P.; Grilli, E.; Amand, T.; Marie, X.; Myronov, M.; Pezzoli, F. Spin-coherent dynamics and carrier lifetime in strained $Ge_{1-x}Sn_x$ semiconductors on silicon. *Phys. Rev. B* **2019**, *99*, 035202.
(37) Julsgaard, B.; von den Driesch, N.; Tidemand-Lichtenberg, P.; Pedersen, C.; Ikonic, Z.; Buca, D. Carrier lifetime of GeSn measured by spectrally resolved picosecond photoluminescence spectroscopy. *Photonics Res.* **2020**, *8*, 788.
(38) Pezzoli, F.; Giorgioni, A.; Patchett, D.; Myronov, M. Temperature-Dependent Photoluminescence Characteristics of GeSn Epitaxial Layers. *ACS Photonics* **2016**, *3*, 2004−2009.
(39) Gippius, A.; Vavilov, V. Radiative recombination at dislocation in Germanium. *Radiative recombination at dislocation in Germanium*; Springer, 1968.
(40) Figielski, T.; Morawski, A. Position and Nature of Electron States Associated with Dislocation in Ge. *Phys. Status Solidi A* **1971**, *6*, 617.
(41) Liu, T.; Wang, L.; Zhu, G.; Hu, X.; Dong, Z.; Zhong, Z.; Jia, Q.; Yang, X.; Jiang, Z. Dislocation-related photoluminescence of GeSn films grown on Ge (001) substrates by molecular beam epitaxy. *Semicond. Sci. Technol.* **2018**, *33*, 125022.
(42) Gupta, S.; Simoen, E.; Loo, R.; Shimura, Y.; Porret, C.; Gencarelli, F.; Paredis, K.; Bender, H.; Lauwaert, J.; Vrielinck, H.; Heyns, M. Electrical properties of extended defects in strain relaxed GeSn. *Appl. Phys. Lett.* **2018**, *113*, 022102.
(43) Takeuchi, W.; Asano, T.; Inuzuka, Y.; Sakashita, M.; Nakatsuka, O.; Zaima, S. Characterization of Shallow- and Deep-Level Defects in Undoped $Ge_{1-x}Sn_x$ Epitaxial Layers by Electrical Measurements. *ECS J. Solid State Sci. Technol.* **2015**, *5*, P3082−P3086.
(44) Nakatsuka, O.; Tsutsui, N.; Shimura, Y.; Takeuchi, S.; Sakai, A.; Zaima, S. Mobility Behavior of $Ge_{1-x}Sn_x$ Layers Grown on Silicon-on-Insulator Substrates. *Jpn. J. Appl. Phys.* **2010**, *49*, 04DA10.
(45) Conley, B. R.; Mosleh, A.; Ghetmiri, S. A.; Du, W.; Soref, R. A.; Sun, G.; Margetis, J.; Tolle, J.; Naseem, H. A.; Yu, S.-Q. Temperature dependent spectral response and detectivity of GeSn photoconductors on silicon for short wave infrared detection. *Opt. Express* **2014**, *22*, 15639.
(46) Zürch, M.; Chang, H.-T.; Borja, L. J.; Kraus, P. M.; Cushing, S. K.; Gandman, A.; Kaplan, C. J.; Oh, M. H.; Prell, J. S.; Prendergast, D.; Pemmaraju, C. D.; Neumark, D. M.; Leone, S. R. Direct and simultaneous observation of ultrafast electron and hole dynamics in germanium. *Nat. Commun.* **2017**, *8*, 15734.
(47) Zhou, X. Q.; van Driel, H. M.; Mak, G. Femtosecond kinetics of photoexcited carriers in germanium. *Phys. Rev. B* **1994**, *50*, 5226−5230.
(48) Mak, G.; van Driel, H. M. Femtosecond transmission spectroscopy at the direct band edge of germanium. *Phys. Rev. B* **1994**, *49*, 16817−16820.
(49) Rappen, T.; Peter, U.; Wegener, M.; Schäfer, W. Coherent dynamics of continuum and exciton states studied by spectrally resolved fs four-wave mixing. *Phys. Rev. B* **1993**, *48*, 4879−4882.
(50) Kaplan, C. J.; Kraus, P. M.; Ross, A. D.; Zürch, M.; Cushing, S. K.; Jager, M. F.; Chang, H.-T.; Gullikson, E. M.; Neumark, D. M.; Leone, S. R. Femtosecond tracking of carrier relaxation in germanium with extreme ultraviolet transient reflectivity. *Phys. Rev. B* **2018**, *97*, 205202.
(51) Tanaka, K.; Ohtake, H.; Suemoto, T. Determination of intervalley scattering time in germanium by subpicosecond time-resolved Raman spectroscopy. *Phys. Rev. Lett.* **1993**, *71*, 1935−1938.
(52) Zollner, S.; Myers, K. D.; Jensen, K. G.; Dolan, J. M.; Bailey, D. W.; Stanton, C. J. Femtosecond interband hole scattering in Ge studied by pump-probe reflectivity. *Solid State Commun.* **1997**, *104*, 51−55.
(53) Syperek, M.; Baranowski, M.; Sęk, G.; Misiewicz, J.; Löffler, A.; Höfling, S.; Reitzenstein, S.; Kamp, M.; Forchel, A. Impact of wetting-layer density of states on the carrier relaxation process in low indium content self-assembled (In,Ga)As/GaAs quantum dots. *Phys. Rev. B* **2013**, *87*, 125305.
(54) Gourdon, C.; Lavallard, P. Exciton Transfer between Localized States in $CdS_{1-x}Se_x$ Alloys. *Phys. Status Solidi B* **1989**, *153*, 641−652.
(55) Rubel, O.; Baranovskii, S. D.; Hantke, K.; Kunert, B.; Rühle, W. W.; Thomas, P.; Volz, K.; Stolz, W. Model of temperature quenching of photoluminescence in disordered semiconductors and comparison to experiment. *Phys. Rev. B* **2006**, *73*, 233201.
(56) Kudrawiec, R.; Syperek, M.; Latkowska, M.; Misiewicz, J.; Korpijärvi, V.-M.; Laukkanen, P.; Pakarinen, J.; Dumitrescu, M.; Guina, M.; Pessa, M. Influence of non-radiative recombination on photoluminescence decay time in GaInNAs quantum wells with Ga- and In-rich environments of nitrogen atoms. *J. Appl. Phys.* **2012**, *111*, 063514.
(57) Baranowski, M.; Kudrawiec, R.; Syperek, M.; Misiewicz, J.; Sarmiento, T.; Harris, J. S. Time-resolved photoluminescence studies of annealed 1.3 μm GaInNAsSb quantum wells. *Nanoscale Res. Lett.* **2014**, *9*, 81.
(58) Schubert, E. F. *Light-Emitting Diodes*; Cambridge University Press, 2006.
(59) Trita, A.; Cristiani, I.; Degiorgio, V.; Chrastina, D.; von Känel, H. Measurement of carrier lifetime and interface recombination velocity in Si−Ge waveguides. *Appl. Phys. Lett.* **2007**, *91*, 041112.
(60) Geiger, R. Direct Band Gap Germanium for Si-compatible Lasing. Diss. ETH No. 23403. Ph.D. Thesis, ETH Zurich, 2016.
(61) Syperek, M.; Dusanowski, Ł.; Andrzejewski, J.; Rudno-Rudziński, W.; Sęk, G.; Misiewicz, J.; Lelarge, F. Carrier relaxation dynamics in InAs/GaInAsP/InP(001) quantum dashes emitting near 1.55 μm. *Appl. Phys. Lett.* **2013**, *103*, 083104.
(62) Jahandar, P.; Weisshaupt, D.; Colston, G.; Allred, P.; Schulze, J.; Myronov, M. The effect of Ge precursor on the heteroepitaxy of $Ge_{1-x}Sn_x$ epilayers on a Si (001) substrate. *Semicond. Sci. Technol.* **2018**, *33*, 034003.
(63) Syperek, M.; Ryczko, K.; Dallner, M.; Dyksik, M.; Motyka, M.; Kamp, M.; Höfling, S.; Misiewicz, J.; Sęk, G. Room Temperature Carrier Kinetics in the W-type GaInAsSb/InAs/AlSb Quantum Well Structure Emitting in Mid-Infrared Spectral Range. *Acta Phys. Pol., A* **2016**, *130*, 1224−1228.
(64) Dusanowski, Ł.; Syperek, M.; Rudno-Rudziński, W.; Mrowiński, P.; Sęk, G.; Misiewicz, J.; Somers, A.; Reithmaier, J. P.; Höfling, S.; Forchel, A. Exciton and biexciton dynamics in single self-assembled InAs/InGaAlAs/InP quantum dash emitting near 1.55 μm. *Appl. Phys. Lett.* **2013**, *103*, 253113.

https://dx.doi.org/10.1021/acsaelm.0c00889
ACS Appl. Electron. Mater. 2021, 3, 344−352